JOURNAL OF MATERIALS SCIENCE **40** (2005) 2013–2021

Solid state characterization of coprecipitated alumina-gallia mixed oxide powders

V. S. ESCRIBANO
Departamento de Química Inorgánica, Universidad de Salamanca, Pl. de la Merced, s/n, E-37008 Salamanca, Spain

J. M. G. AMORES
Departamento de Química Inorgánica, Lab. Complutense de Altas Presiones, Universidad Complutense, Ciudad Universitaria, E-28040 Madrid, Spain

E. F. LÓPEZ
Departamento de Química Inorgánica, Universidad de Salamanca, Pl. de la Merced, s/n, E-37008 Salamanca, Spain

M. PANIZZA, C. RESINI
Departamento de Química Inorgánica, Lab. Complutense de Altas Presiones, Universidad Complutense, Ciudad Universitaria, E-28040 Madrid, Spain

G. BUSCA*
Dipartimento di Ingegneria Chimica e di Processo, Università di Genova, P.le Kennedy 1, I-16129 Genova, Italy
E-mail: Guido.Busca@unige.it

Powders with composition $(Al_xGa_{1-x})_2O_3$ (x = 0, 0.25, 0.50, 0.75, 1) have been prepared by coprecipitation from aluminum nitrate and gallium nitrate and have been charaterized after drying at 373 K and calcination at 673, 1073 and 1473 K, using XRD, DTA, FT-IR and diffuse reflectance UV-VIS and BET surface area and porosity measurements. At 373 K Al compounds are essentially amorphous and for the $Ga_{0.75}$ $Al_{0.25}$ sample a solubility of 12% of Al^{3+} in the diaspore type α-GaOOH has been calculated. In samples calcined at 673 and 1073 K for the Al-rich ones a poorly crystalline defective spinel-type phase γ-Al_2O_3 has been found while the Ga-rich materials are composed of the metastable corundum type phase α-Ga_2O_3 and the thermodynamically β-Ga_2O_3 at 673 and 1073 K respectively. Al^{3+} added to α-Ga_2O_3 tends to hinder the $\alpha \rightarrow \beta$ phase transition of gallium oxide. At 1473 K mixed oxides give rise the thermodynamically stable α-Al_2O_3 and β-Ga_2O_3 phases. Reciprocal solubilities of Ga and Al in their oxides have been calculated.

1. Introduction

At least three polymorphs of gallium oxide are reported and largely described in the literature. In contrast to what happens for the oxides of other trivalent elements such as Al, Fe and Cr sesquioxides, the corundum type hexagonal phase α-Ga_2O_3, which is fequently reported to be formed at low temperature [1, 2], is not thermodynamically stable. The "disordered" cubic defective spinel γ-Ga_2O_3 is also reported to exist as a metastable phase [3] and considered to be isostructural with γ-Al_2O_3. The thermodynamically stable form of gallia is β-Ga_2O_3 [4, 5], whose structure derives from a defective spinel structure but cations and vacancies are ordered and monoclinic distortion occurs. β-Ga_2O_3 is isostructural with θ-Al_2O_3, which is, in contrast, a metastable form of alumina. Gallium oxide has been proposed as a main component of gas sensors due to its semiconducting properties [6, 7], as transparent conductor [8, 9] and as a phosphor due to its luminescent properties [10].

Alumina gallia mixed oxides are today the object of increasing interest in the field of heterogeneous catalysis. They have in fact been reported to be excellent catalysts for the selective catalytic reduction of nitrogen oxides by methane [11] and for alkane selective dehydrogenation [12–15]. According to high-temperature studies, the solubility of gallia in corundum is limited to less than 20% at/at, while the solubility of alumina in β-$Ga_2O_3$is larger, up to more than 70% at/at [16]. On the other hand, most of alumina-gallia systems used in

*Author to whom all correspondence should be addressed.

catalysis are prepared by impregnation (i.e., are constituted by alumina-supported gallia) or are poorly crystalline gamma-type phases.

Following a systematic study on mixed oxides of trivalent elements prepared in powder form, we investigated recently the Ga_2O_3/Fe_2O_3 [17] and the Ga_2O_3/Mn_2O_3 systems [18]. We previously found that a complete solubility exists between α-Ga_2O_3, and α-Fe_2O_3, but that the corundum type solid solutions convert into β-Ga_2O_3-type solid solutions for Ga rich compositions, while they are stable in the alpha form for Fe rich compositions. Interestingly, the equimolar composition is a monophasic alpha-phase at 673 K, splits into an alpha phase and a beta phase at 1073 K and is again monophasic with the perovskite $GaFeO_3$ structure at 1273 K. In the case of the Ga_2O_3/Mn_2O_3 system we found that the presence of Mn ions tends to favor the formation of the β-Ga_2O_3 phase also at low temperature and that a large solubility of Mn^{3+} in this phase occurs with a decrease of the cell volume. In contrast, the presence of Ga^{3+} tends to favor the formation of the spinel Mn_3O_4 with respect to Bixbyite α-Mn_2O_3.

To complete our investigation on the mixed oxides of trivalent elements, we reconsidered the Ga_2O_3/Al_2O_3 system which has already been the object of several studies.

2. Experimental

Al-Ga mixed oxides, denoted as $(Al_xGa_{1-x})_2O_3$ (with $x = 0$, 0.25, 0.50, 0.75 and 1), have been prepared by a coprecipitation method from $Al(NO_3)_3\ 9H_2O$ and $Ga(NO_3)_3{\cdot}9H_2O$, adding ammonium hydroxide until pH $\sim$ 8, then aged for 24 h under continuous stirring and gentle heating, washed with distilled water, dried overnight at 373 K and milled. Portions of each sample were taken and calcined for 3 h at 673, 1073, 1473 K in a Nabertherm furnace.

The XRD analyses have been performed on a Siemens D-500 Diffractometer (Cu K radiation, Ni filter; 30 mA, 40 kV) equipped with the Diffract AT V3 software package. Cell parameters were calculated with a dedicated least square software. Particle size were calculated according to the Scherrer formula [19].

DTA analyses were performed in dynamic air atmosphere from 298 to 1373 K with heating rates of 10 K/min on a Perkin Elmer DTA instrument.

FT-IR spectra were recorded in the range 4000–400 cm^{-1} with a Nicolet Avatar 360 spectrometer using the KBr dilution technique. DR-UV-Vis spectra were obtained with a Shimazdu 2401 PC instrument with a $BaSO_4$ reference.

Specific surface areas were measured by N_2 adsorption at the liquid nitrogen temperature (77 K) on a conventional volumetric apparatus according to the BET method. From the desorption branch of the isothermal representation, the pore size distribution was estimated by the BJH method [20].

3. Results

3.1. Characterization of the precipitates

The structural parameters of the precipitates, together with those of the calcined oxides are summarized in Table I. Chemical analyses, performed on the oxides calcined at 1073 K, provide evidence for the presence of an excess of Al with respect to the nominal ones in all mixed preparations.

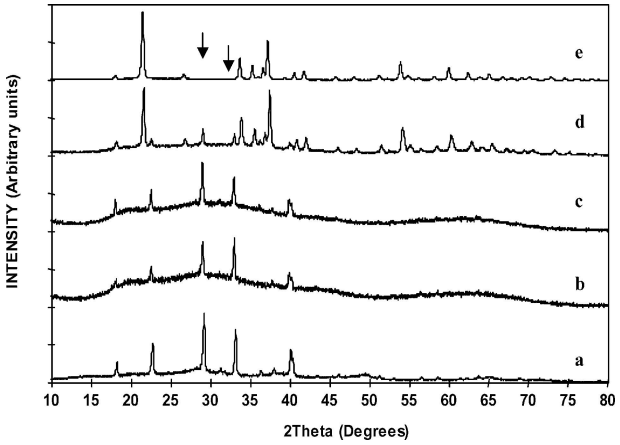

Figure 1 XRD patterns of the precipitates: (a) Al_1Ga_0, (b) $Al_{0.75}Ga_{0.25}$, (c) $Al_{0.50}Ga_{0.50}$, (d) $Al_{0.25}Ga_{0.75}$, and (e) Al_0Ga_1.

In all XRD patterns of the precipitate, sharp diffraction peaks characteristic of ammonium nitrate (ICDD file no 8-0452) are observed in all case except Ga. In the XRD patterns of the pure Ga and $Ga_{0.75}Al_{0.25}$ materials, Fig. 1, the α-GaOOH phase (Diaspore-type, ICDD file no 26-0674) is observed, whereas Al-rich precipitates are amorphous in all samples. Calculated cell parameters for the α-GaOOH phase decrease slightly in the mixed material, which indicates the formation of a solid solution of Al^{3+} ions into the Ga hydroxide. According to Vegard's law [21] and the literature cell parameters of pure α-AlOOH (diaspore) a solubility of 12% is calculated from a parameter. This value is notably lower than the Al content of this sample, which indicates that an amorphous (XRD undetected) Al compound also segregates as an additional phase.

The overall aspect of the FT-IR spectra for these materials (Fig. 2) is rather complex due to the large amount of different species present. However, some considerations can be made. Thus, bands appearing above 2800 cm^{-1} (not shown) are characteristic of stretching modes of NH_4^+ and OH species. A very intense band at about 1390 cm^{-1} and another sharp one at 830 cm^{-1} are assigned to the ν(NO) and δ(ONO) modes of nitrate groups, respectively, according to the presence of ammonium nitrate in the samples. A sharp band at 1720 cm^{-1} is attributed to the symmetric deformation mode of ammonium cations, $\delta_{sy}(NH_4^+)$. The main differences among the spectra are found in the region below 1200 cm^{-1} characteristic of MO and OH lattice vibrations in the oxo-hydroxides.

Thus, in the spectrum of the pure Al sample (Fig. 2a) absorptions at 740, 614 and 480 cm^{-1} are in complete agreement with those reported in literature for a complex Al and ammonium hydroxide precipitates [22]. The higher number of the OH in plane deformation bands (appearing here at 1070, 1051, 970 and 890 cm^{-1}) and their shifts with respect to those in the reference work are probably due to the different composition of the Al hydroxide.

TABLE I Structural characteristic of the Al-Ga samples

Sample	T (K)	Al/Ga atomic ratio	Phases	Cell parameters (Å)			Volume (Å^3)	Crystal size (Å)
				a	*b*	*c*		
Al_1Ga_0	As obtained		amorphous					
$Al_{0.75}Ga_{0.25}$			amorphous					
$Al_{0.50}Ga_{0.50}$			amorphous					
$Al_{0.25}Ga_{0.75}$			amorphous GaOOH	4.5493	9.7548	2.9531	131.05	334
Al_0Ga_1			GaOOH	4.5695	9.8105	2.9734	133.29	279
Al_1Ga_0	673		γ-Al_2O_3					
$Al_{0.75}Ga_{0.25}$			γ-Al_2O_3					
$Al_{0.50}Ga_{0.50}$			γ-Al_2O_3					
$Al_{0.25}Ga_{0.75}$			α-Ga_2O_3	4.9568		13.3677	284.44	171
Al_0Ga_1			α-Ga_2O_3	4.9787		13.4322	288.34	190
Al_1Ga_0	1073	∞	γ-Al_2O_3	7.9028			493.56	94
$Al_{0.75}Ga_{0.25}$		3* 4.48$^+$	γ-Al_2O_3	7.9439			501.30	70
$Al_{0.50}Ga_{0.50}$		1* 1.61$^+$	γ-Al_2O_3	8.0222			516.27	67
$Al_{0.25}Ga_{0.75}$		0.33* 0.53$^+$	β-Ga_2O_3	12.1892	3.0199 (103.96)	5.7886	206.78	244
			α-Ga_2O_3					364
Al_0Ga_1		0	β-Ga_2O_3	12.2604	3.0326 (103.77)	5.8077	209.72	260
Al_1Ga_0	1473		α-Al_2O_3	4.7558		12.9741	254.13	546
$Al_{0.75}Ga_{0.25}$			α-Al_2O_3 β-Ga_2O_3	4.7861		13.0400	258.68	592
$Al_{0.50}Ga_{0.50}$			β-Ga_2O_3	11.5951	2.9892 (106.29)	5.8854	195.80	478
$Al_{0.25}Ga_{0.75}$			β-Ga_2O_3	12.0086	3.0006 (103.78)	5.7294	200.51	401
Al_0Ga_1			β-Ga_2O_3	12.1905	3.0439 (103.75)	5.7888	208.64	462

NH_4NO_3 (ICDD file no 8-0452): $a = 4.942$ $b = 5.438$ $c = 5.745$ (Orthorhombic).
GaOOH (ICDD file no 6-0180): $a = 4.580$ $b = 9.800$ $c = 2.970$ (Orthorhombic).
γ-Al_2O_3 (ICDD file no 29-0063): $a = 7.924$ (Cubic).
α-Ga_2O_3 (ICDD file no 74-1610): $a = 4.9825$ $c = 13.4330$ (Rhombohedral).
β-Ga_2O_3 (ICDD file no 76-0573): $a = 12.2300$ $b = 3.0400$ $c = 5.8000$ $\beta = 103.7$ (Monoclinic).
α-Al_2O_3 (ICDD file no 82-1468): $a = 4.7589$ $c = 12.9919$ (Rhombohedral).
θ-Ga_2O_3 (ICDD file no 35-0121): $a = 5.620$ $b = 2.906$ $c = 11.790$ $\beta = 103.79$ (Monoclinic).
(*) Nominal atomic ratio.
($^+$) Experimental atomic ratio.

When Ga is added up to a 50% limit (Fig. 2b and c) the component at 740 cm^{-1} gradually shifts to 707 cm^{-1} and that at 614 cm^{-1} increases greatly in intensity and shifts to 555 cm^{-1}, whereas at 480 cm^{-1} completely disappears. These facts probably evidence the partial solubility of Ga into the amorphous Al hydroxide phase. In parallel, a broad band develops at 953 cm^{-1} with a shoulder at 1050 cm^{-1}: these bands probably evidence the beginning of the crystallization of the oxyhydroxide phase. The features in the vibrational spectra change dramatically by further addition of Gallium. Thus, the spectrum for the pure sample (Fig. 2e) displays absorption bands at 1011, 954, 690, 640, 506 and 415 cm^{-1}, in very good agreement with those reported in literature for the α-GaOOH phase [23, 24]. The spectrum for the mixed sample $Al_{0.25}Ga_{0.75}$ (Fig. 2d) is much less resolved due to the partial replacement of Ga^{3+} cations by Al^{3+} ones within the GaOOH lattice and the likely presence of amorphous material.

An extensive discussion on the predicted vibrational modes for an α-MOOH compound with goethite or diaspore structure (orthorhombic unit cell, in space group $Pbnm = D_{2h}^{16}$ (no 62), Z = 4) has been reported by Gallardo Amores *et al.* [25] as well as in previous studies [26, 27]. According to that work, we propose all of our samples are composed by goethite like compounds, being the shifts in the bands due to the different electronegativities of Al and Ga and bond lengths (neglecting the effects of particle aggregations). The bands below 750 cm^{-1} are related to MO stretches of MO_6 octahedra; those in the range 950–1100 cm^{-1} to in plane OH deformation modes.

DTA curves recorded in air for the precipitates previously dried at 100°C are shown in Fig. 3. The Ga-free and mixed precipitates (Fig. 3a–d) present a broad endothermic step in the range 100–260°C, attributed to desorption of adsorbed water, NH_3 and NO_x species, and then a very intense and sharp exothermic peak at 300°C for the pure Al sample and shifted to lower temperature (280°C) for the mixed samples. According to literature data [28] and XRD analyses, that is associated with the NH_4NO_3 decomposition. In the case of the $Al_{0.25}Ga_{0.75}$ and Al-free compounds (Fig. 3d and e) a clear endothermic peak is observed at 420 and 410°C respectively, assigned to oxyhydroxide α-GaOOH decomposition give rise to α-Ga_2O_3 [22]. These data show that Al^{3+} tends to hinder the α-GaOOH to α-Ga_2O_3phase transition.

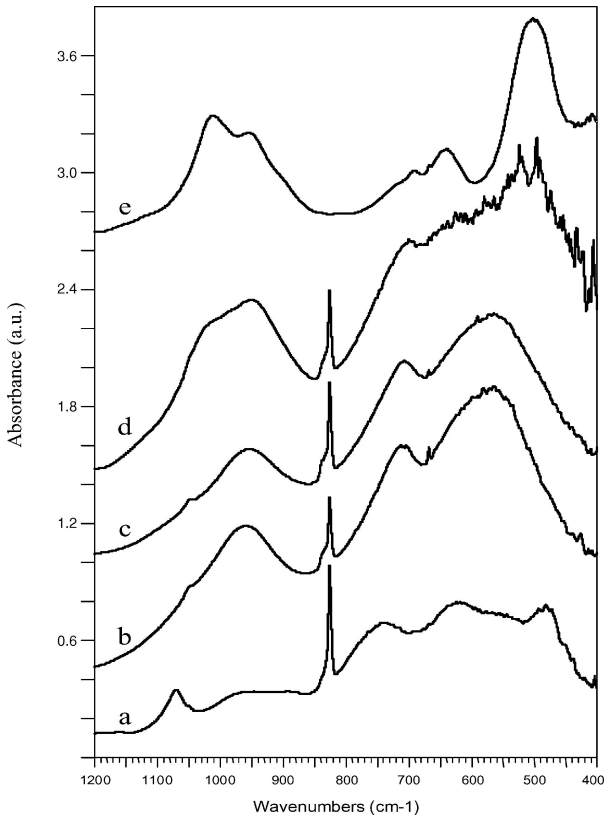

Figure 2 FT-IR spectra of the precipitates: (a) Al_1Ga_0, (b) $Al_{0.75}Ga_{0.25}$, (c) $Al_{0.50}Ga_{0.50}$, (d) $Al_{0.25}Ga_{0.75}$, and (e) Al_0Ga_1.

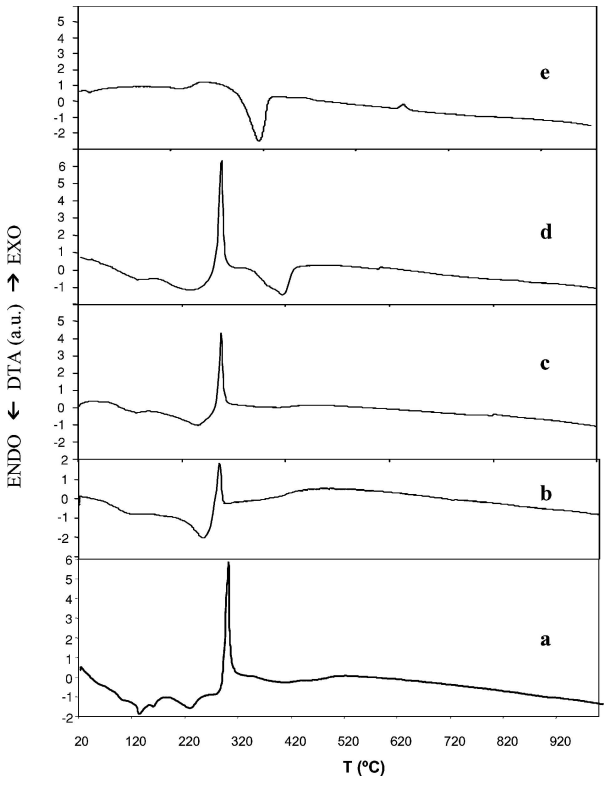

Figure 3 DTA curves of precipitates powders: (a) Al_1Ga_0, (b) $Al_{0.75}Ga_{0.25}$, (c) $Al_{0.50}Ga_{0.50}$, (d) $Al_{0.25}Ga_{0.75}$, and (e) Al_0Ga_1.

The DTA curve relative to the Ga pure sample (Fig. 3e) show a quite different picture. In fact, the sample after drying appears like α-GaOOH phase, which decomposes to metastable form α-Ga_2O_3 at 410°C K. Finally a weak exothermic feature is detected at 720°C,

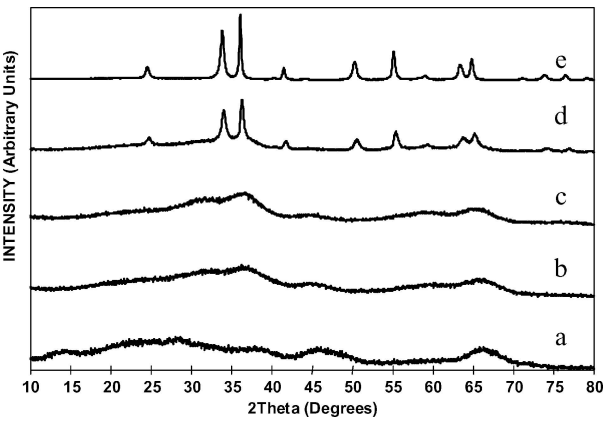

Figure 4 XRD patterns of the oxides calcined at 673 K: (a) Al_1Ga_0, (b) $Al_{0.75}Ga_{0.25}$, (c) $Al_{0.50}Ga_{0.50}$, (d) $Al_{0.25}Ga_{0.75}$, and (e) Al_0Ga_1.

which is associated with the phase transition from α-Ga_2O_3 toward its thermodynamically stable form, β-Ga_2O_3.

3.2. Characterization of the mixed oxides

3.2.1. XRD

The X-ray diffraction patterns of the samples calcined at 673 K are shown in Fig. 4. The broad features in the patterns for the Al-rich materials (Fig. 4a–c) correspond to a poorly crystalline defective spinel-type phase γ-Al_2O_3 [29, 30] (ICDD file no 29-0063). The Ga-rich materials (Fig. 4d and e) are, conversely, highly crystalline and are composed of the corundum type phase α-Ga_2O_3 (ICDD file no 74-1610). Its characteristic reflections are notably shifted towards higher d-spacings for $Ga_{0.75}Al_{0.25}$ in the mixed sample (with the respect to the pure one) according to the dissolution of Al^{3+} cations within the corundum type structure. The solubility calculated with Vegard's law from the *a* parameter is 10%, the value calculated from *c* parameter is slightly higher (15%). Both values are significantly lower than the experimentally measured Al content in the sample, which suggests co-presence of another Al-rich amorphous phase in order to fulfill the nominal composition of the material. No additional peaks characteristic of a long range arrangement of Al^{3+} and Ga^{3+} cations in the solution phase are detected in the diffraction pattern of the $Al_{0.25}Ga_{0.75}$ sample (Fig. 4d), which indicates that the replacement of both cations is random.

In Fig. 5 the diffraction patterns of the oxides calcined at 1073 K are reported. In those of Al-rich materials (Fig. 5a–c) γ-Al_2O_3 appears as only phase with a slightly higher degree of crystallinity than in the samples calcined at 673 K. No traces of other alumina varieties, like θ or η, are detected both in the pure and the mixed samples. An increasing of the *a* cell parameter (Table I) and consequently a systematic shift of the reflections to higher d-spacings is observed upon increasing the Ga-content, according to the difference between the ionic radii of Al^{3+} and Ga^{3+} (0.50 and 0.62 Å, respectively). This fact indicates that Ga enters the spinel-type structure in a substitutional solid solution. The pure Ga sample (Fig. 5e) is composed of the thermodynamically stable β-Ga_2O_3 phase (ICDD file

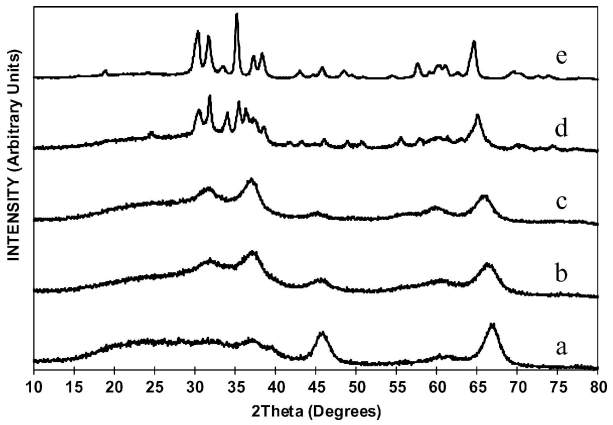

Figure 5 XRD patterns of the oxides calcined at 1073 K: (a) Al_1Ga_0, (b) $Al_{0.75}Ga_{0.25}$, (c) $Al_{0.50}Ga_{0.50}$, (d) $Al_{0.25}Ga_{0.75}$, and (e) Al_0Ga_1.

no 76-0573). Doping with Al^{3+} (Fig. 5d) results in the minority formation of the α-Ga_2O_3, evidencing the inhibiting effect of Al on the thermodynamically driven $\alpha \rightarrow \beta$ phase transition of gallium oxide. An analogous behavior has been previously reported for the Fe_2O_3-Ga_2O_3 system [14]. A solid solution of Al^{3+} is also formed for the β variety as deduced from the shifts of its reflection peaks to higher d-spacings in the pattern for the $Ga_{0.75}$ $Al_{0.25}$ mixed sample (Fig. 5d). Vegard's law has been applied taking as a reference for θ-Al_2O_3 the ICDD card no 35-0121 (monoclinic symmetry, space group A2/m [12]). Thus, a value of 15% of Al^3into β-Ga_2O_3 is calculated. It must be also taken into account that the α-phase observed in the same graphic very likely corresponds to a $(Al, Ga)_2O_3$ composition. Therefore, the solubility of Al into Ga oxide definitely increases at 1073 K.

At 1473 K aluminum oxide has undergone the $\gamma \rightarrow \alpha$ structural transition. It is detected for Ga-content up to 25% (Fig. 6a and b). The unit cell of α-Al_2O_3 (ICDD file no 82-1468) expands upon adding Ga, evidencing the formation of a solid solution phase. Solubility calculated from *a* parameter is approximately 14%. On the other hand, β-Ga_2O_3 is the only gallium oxide detected in all samples up to a 75% Al composition (Fig. 6c–e). This agrees with the high temperature data reported by Mizuno *et al*. [13].

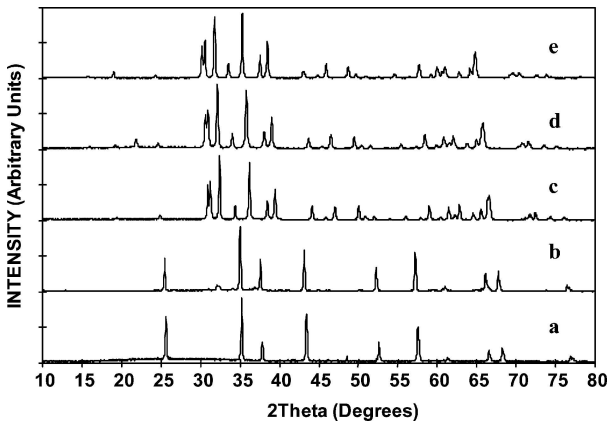

Figure 6 XRD patterns of the oxides calcined at 1073 K: (a) Al_1Ga_0, (b) $Al_{0.75}Ga_{0.25}$, (c) $Al_{0.50}Ga_{0.50}$, (d) $Al_{0.25}Ga_{0.75}$, and (e) Al_0Ga_1.

The solubility of Al into this phase, evaluated from the Vegard's law, is almost total (31%) in the sample $Al_{0.25}Ga_{0.75}$ and reaches a limit of 40% in the $Al_{0.50}Ga_{0.50}$sample. These data show that reciprocal solubilities are strongly enhanced by increasing the treatment temperature. Opposite to the Ga-Fe [14] system, no binary compounds are obtained by high temperature reaction between Al and Ga oxides, in agreement again to previous studies [16].

3.2.2. Skeletal FT-IR spectroscopy

The vibrational spectra of the samples calcined at 673 K are compared in the range 1200–400 cm^{-1} in Fig. 7. That for the pure Al sample (Fig. 7a) is typical of γ-alumina [31, 32], in agreement with XRD data. It displays a broad absorption in the region 500–1000 cm^{-1}, which is characteristic of aluminas with spinel related structures [11, 33] and it is assigned to AlO_4 tetrahedra [34]. Components are located at approximately 480 (sh), 615 (maximum), 735 (sh) and 900 cm^{-1} (sh). An additional band at about 1070 cm^{-1}, which is not detected in the other samples of the series, could be related to the presence of traces of Al hydroxide not detected by XRD analyses. When Ga^{3+} is added up to 50% limit (Fig. 7b and c), the spectra become more unresolved and the bands tend to shift to lower wavenumbers. The same effect has been reported for related systems [3, 35] and is attributed to the dissolution of Ga^{3+} into alumina.

On the other side of the compositional range, the spectrum of the pure Ga sample (Fig. 7e) displays

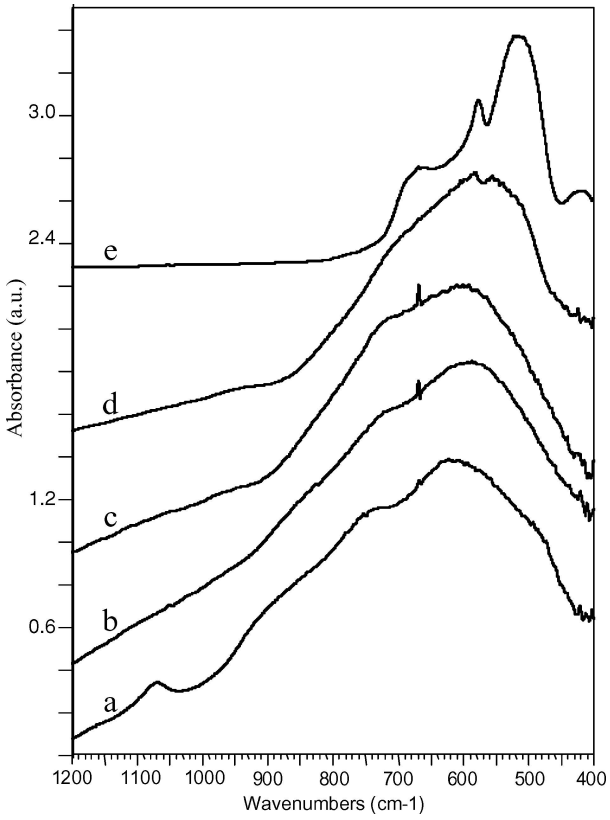

Figure 7 FT-IR spectra of the oxides calcined at 673K: (a) Al_1Ga_0, (b) $Al_{0.75}Ga_{0.25}$, (c) $Al_{0.50}Ga_{0.50}$, (d) $Al_{0.25}Ga_{0.75}$, and (e) Al_0Ga_1.

absorptions at 420, 515, 577, 660 cm^{-1}. According to XRD analyses, it corresponds to the α-Ga_2O_3 phase. The hexagonal-rhombohedral α-M_2O_3 compounds crystallize in the $D^6_{3d} = R\bar{3}c$ group with two formula units per unit cell [1]. The analysis of the factor group predicts six IR-active fundamental modes [36]. However, the interpretation of skeletal IR spectra of powders is complex due to the sensitivity to crystal shape, particles aggregation and matrix material. By comparison with the spectra of single crystals of α-Al_2O_3 [37] and α-Fe_2O_3 [38] as well as powder samples [15] the following assignment of the bands in the spectrum of α-Ga_2O_3 is proposed: ν_4 (symmetry E_u) at 420 cm^{-1}, ν_5 (E_u) at 515 cm^{-1}, ν_2 (A_{2u}) at 577 cm^{-1}, ν_6 (E_u) at 660 cm^{-1}.

The spectrum of the mixed oxide containing 25% nominal Al (Fig. 7d) is much less resolved and displays a broad absorption at higher wavenumbers, i.e. up to 950 cm^{-1}. We attribute the latter feature to the co-presence of a spinel-type Al-rich phase which escapes XRD analyses rather than to fundamental modes in particle with extreme morphologies. However, the solid solution α-$(Al,Ga)_2O_3$ phase must be still present as the maximum of the main absorption falls very close to that of the α-Ga_2O_3.

The skeletal spectra of the Al-rich samples calcined at 1073 K (Fig. 8a–c) are very similar to those of the samples calcined at 673 K. That for the pure sample (Fig. 8a) displays a broad absorption in the region 500–950 cm^{-1} and is typical of γ-Al_2O_3, though the main maximum is shifted to 560 cm^{-1} and the shoulder near 500 cm^{-1} is more pronounced maybe as a result of the enhanced crystallinity or to higher homogeneity in the morphology of the material. When Ga^{3+} is added (Fig. 8b and c), the features in the spectra shift slightly downfield according to the formation of the solid solution of Ga^{3+} cations in the corundum type structure. Further addition gallium leads to dramatic changes in the spectra. Thus, that for the gallium pure sample (Fig. 8e) displays absorptions at 755, 685 and 476 cm^{-1} and is in good agreement with those reported in literature for β-Ga_2O_3 [39, 40]. The components in the region 400–600 cm^{-1} correspond to bending vibrations whereas those above 600 cm^{-1} are assigned to GaO_4 tetrahedral stretching modes [20]. In the spectrum of the $Al_{0.25}Ga_{0.75}$ sample (Fig. 8d), the bands are significantly shifted to higher wavenumbers and broadened due to the formation of the a random solid solution of Al^{3+} in β-Ga_2O_3. The enlargement of the absorption at to 900 cm^{-1} points out the co-presence of the corundum type structure detected by XRD.

3.2.3. Electronic spectra

The electronic spectra of the oxides calcined at 673 K are shown in Fig. 9. That of the pure Al sample (Fig. 9a) displays an absorption edge below 240 nm with a maximum 210 nm and residual absorption up to 320 nm. No transitions in the visible region are observed due to the $2s^2p^6$ configuration of Al^{3+}. According to literature, this spectrum is characteristic of γ-Al_2O_3 and the energy gap calculated (5.18 eV) is very close to that previously reported [41]. γ-Al_2O_3 has a defective spinel structure which Al^{3+} cations present both octahedral and tetrahedral coordination. Thus, the main band in the spectrum is related to $O^{2-} \rightarrow Al^{3+}$ charge transfer transitions and the residual absorption at higher wavelengths might be related to the low crystallinity of the sample. When a 25% gallium is added (Fig. 9b), a more pronounced maximum shifts slightly to lower energies is observed and the residual absorption next to the main component increases moderately. These facts evidence

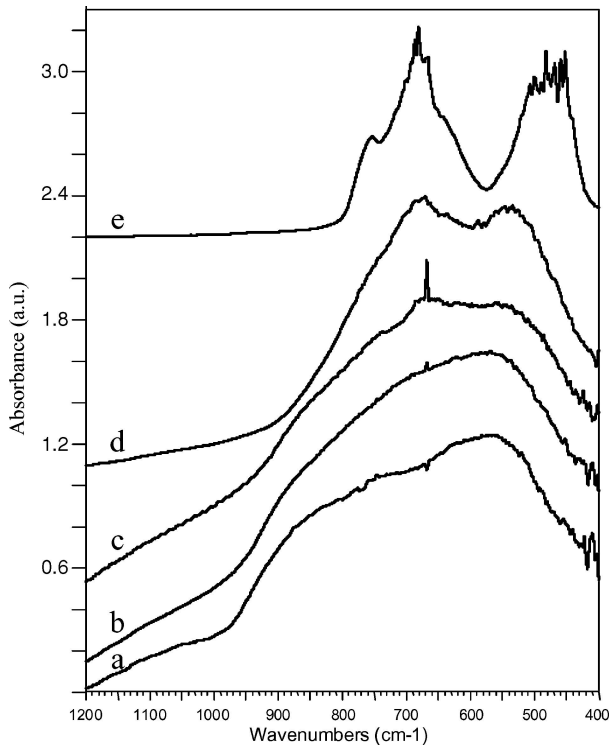

Figure 8 FT-IR spectra of the oxides calcined at 1073: (a) Al_1Ga_0, (b) $Al_{0.75}Ga_{0.25}$, (c) $Al_{0.50}Ga_{0.50}$, (d) $Al_{0.25}Ga_{0.75}$, and (e) Al_0Ga_1.

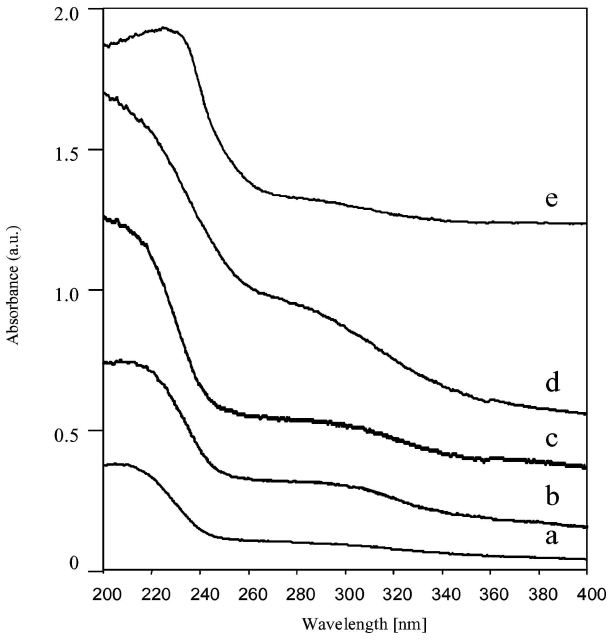

Figure 9 DR-UV spectra of the oxides calcined at 673K: (a) Al_1Ga_0, (b) $Al_{0.75}Ga_{0.25}$, (c) $Al_{0.50}Ga_{0.50}$, (d) $Al_{0.25}Ga_{0.75}$, and (e) Al_0Ga_1.

the formation of a solid solution phase, which results in the distortion of the structure (as observed by XRD).

On the other side of the compositional range, the spectrum of the pure gallium sample (Fig. 9e), composed after XRD by the α-Ga_2O_3 phase, exhibits an absorption edge centered at 230 nm together with a weak absorption tail at higher wavelengths. In the corundum structure of α-Ga_2O_3, gallium ions occupy only octahedral holes. A discussion on the dependence on the symmetry of charge transfer transitions in zirconia polymorphs (one of which has a cubic structure with the metal in octahedral coordination, as the corundum structure) has been previously published [42]. According to the reference work, and assuming that bonding in gallium oxide is mainly ionic, the main band in the spectrum is attributed to a charge transfer transition from approximately the 2p level of O^{2-} to the e_g shell of Ga^{3+}. Doping with Al (Fig. 9c and d) gives rise to the shift of the absorption maximum below 200 nm (i.e. beyond our detection range) and to a systematic strong enhancement of a second component at higher wavelengths. All these facts can be interpreted on the basis of the significantly lower crystallinity of the solid solution phase of Al into β-Ga_2O_3. The notorious shift in the position of the main band must be due to a great distortion of the structure and electronic distribution when Al^{3+} enters the lattice and the occurrence of the second component is related to the loss of the degeneracy of the molecular levels subsequent to the change to a lower symmetry form [22].

The spectra of the oxides calcined at 1073 K (reported in Fig. 10) follow a more definite trend. In that of pure Al sample (Fig. 10a), composed after XRD of the defective spinel γ-Al_2O_3, the main band due to $O^{2-} \rightarrow Al^{3+}$ charge transfer transitions falls now below 200 nm and only residual absorption is observed throughout the UV region. These changes are likely related to the presence of small amounts of transitional aluminas (like θ- or δ-Al_2O_3) not detected by XRD. In fact, the energy gap of alumina increases systematically as long as the $\gamma \rightarrow \alpha$ phase transition occurs. Typical values reported in literature are about 7 eV for γ-Al_2O_3 and 8.8 eV for corundum [21]. Addition of gallium (Fig. 10b and c) results in shifting both the absorption edge and tail to lower energies due to lower crystallinity and to the formation of the solid solution phase. The spectrum of the pure gallium sample (Fig. 10e) displays a broad absorption band below 270 nm. The differences with respect to the pure material calcined at 673 K (Fig. 9e) are probably due to that in the former Al^{3+} exists in both tetrahedral and octahedral coordination (in fact, tetrahedral coordination is predominant). The spectrum of the $Al_{0.25}Ga_{0.75}$ sample (Fig. 10d) is dramatically changed, as the absorption tail above 270 nm increases significantly in intensity. That is attributed mainly to the formation of a very distorted corundum type α-$(Al,Ga)_2O_3$ solid solution phase detected by XRD, as previously explained.

These spectra clearly evidence that the formation of solid solution greatly change the electronic properties of the materials with respect to the pure phases. This is specially stressed in the case of the Al-doped gallium oxides.

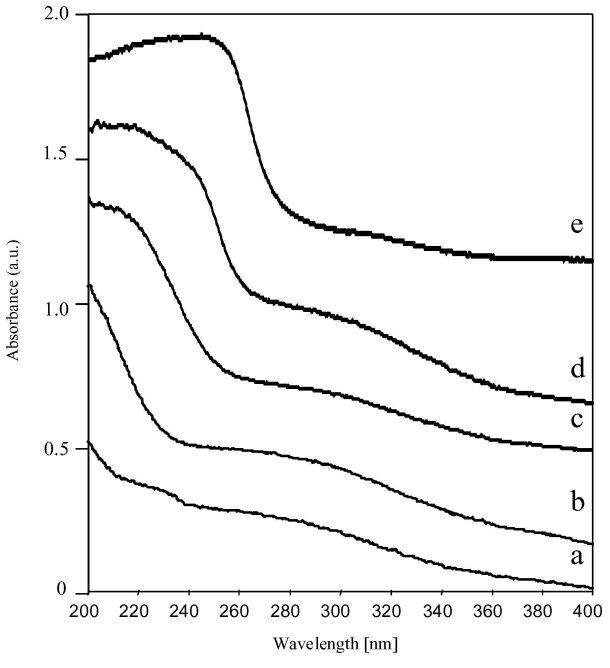

Figure 10 DR-UV spectra of the oxides calcined at 1073 K: (a) Al_1Ga_0, (b) $Al_{0.75}Ga_{0.25}$, (c) $Al_{0.50}Ga_{0.50}$, (d) $Al_{0.25}Ga_{0.75}$, and (e) Al_0Ga_1.

3.2.4. Specific surface area trend

The morphological characteristics of the samples calcined at 673 and 1073 K are compared in Table II. The mixed oxides calcined at 673 K present relatively high specific surface areas in the range 150–230 m^2/g, except the pure gallium sample, whose surface area is notably lower (50 m^2/g) according to its high crystallinity. The addition of gallium to alumina results in a moderate decrease of the pore volume available to the gas (from 227 to about 170 m^2/g), in spite of the lower crystallinity of the solid solution phases, as observed by XRD.

The isothermal plots of the pure Al and Ga samples (not shown here) correspond to the type IV of the BDDT classification [43], characteristic of non porous or macroporous materials, with an H2-type (according to the IUPAC classification) hysteresis loop which is typical of most inorganic oxides with undefined pore sizes distributions and shapes. When gallium is added up to 50% limit, the hysteresis loop tends to disappear

TABLE II Morphological characteristics of the samples calcined at 773 and 1073 K

Sample	Temperature (K)	Surface area (m^2/g)	Pore volume (ml/g)	Pore mean diameter (nm)
Al_1Ga_0	673	227	0.14	1.68
$Al_{0.75}Ga_{0.25}$		157	0.08	0.63
$Al_{0.50}Ga_{0.50}$		167	0.06	1.08
$Al_{0.25}Ga_{0.75}$		171	0.09	1.60
Al_0Ga_1		50	0.11	1.56
Al_1Ga_0	1073	147	0.19	2.09
$Al_{0.75}Ga_{0.25}$		98	0.07	1.61
$Al_{0.50}Ga_{0.50}$		108	0.11	1.61
$Al_{0.25}Ga_{0.75}$		64	0.07	1.71
Al_0Ga_1		24	0.03	2.05

(according to the lower surface area of the samples) and the isothermal profiles turn consequently into the type II, associated to low-porosity absorbents.

Calcination at 1073 K gives rise to a decrease in the specific surface areas, as expected, and now range from 147 m^2/g for the pure Al sample to 24 m^2/g for the pure Ga one. The areas of the mixed materials follow the same trend as above, i.e. they decrease with respect to the pure Al sample but they are significantly higher than that of the pure Ga sample. A moderate shift of the pore mean diameter to higher values (1.60–2.10 nm) is also observed.

The isothermal plots correspond to the type IV of the BDDT with an H2-type hysteresis loop except for the pure gallium sample which present an profile II.

4. Conclusions

The data reported above show that Al compound precipitates and dried at 373 K are essentially amorphous in all samples, whereas in the pure Gallium and $Ga_{0.75}Al_{0.25}$ materials The diaspore-type phase GaOOH is observed. In the mixed sample Al^{3+} into the Ga hydroxyde gives rise a solid solution.

The samples calcined at 673 K correspond to a poorly crystalline defective spinel-type phase γ-Al_2O_3 for the Al-rich compounds and a metastable corundum-type phase α- $Ga_2O_3$for the Ga-rich ones. By calcination at 1073 K γ-$Al_2O_3$is also observed as only phase with a slightly higher degree of crystallinity than in those calcined at 673 K, while the pure Ga sample is composed of the thermodynamically stable β-Ga_2O_3phase. The addition of aluminum (25% at/at) results in the stabilization of $\alpha \rightarrow \beta$ phase transition of gallium oxide but a minority formation of the α-$Ga_2O_3$is detected.

Calcination at 1474 K pure and mixed oxides give rise the thermodynamically stable α-Al_2O_3 and β-Ga_2O_3 phases. Gallium and Aluminum prove a reciprocal solubility in their oxide and hydroxydes compounds. The nominally 1:1 oxide, which has a significant excess of Al (Al/Ga a.r. 1, 6) still is detected as β-Ga_2O_3, θ-Al_2O_3 phase

The specific surface areas of the pure Al and mixed oxides calcined up to 1073 K are characteristic of mesoporous materials, thus present relatively high specific surface area due to the poorly crystalline defective spinel-type phase γ-Al_2O_3 presence. The addition of gallium to alumina generally results in a decrease of the surface area values, becoming for the pure Ga notably lower than those, according to its high crystallinity.

Acknowledgements

This work has been supported in part by Spanish Ministerio de Ciencia y Tecnología (ref. Mat 2000-1113) and INFM (Genoa, Italy). E.F.L., M.P and V.S.E. acknowledge J.C.y L (Spain), University of Genoa (Italy) and Ministerio E.C. y D. (ref. PR2003-0096) respectively.

References

1. B. G. HYDEN and S. ANDERSON, "Inorganic Crystal Structures" (Wiley, New York, 1989).
2. W. PIES and A. WEISS, in "Landolt-Börnstein Zahlenwerte und Funktionen aus Naturwissenschaften und Technik," edited by V. K. H. Hellwege and A. M. Hellwege (Springer, Berlin, 1975) Vol. III/7b.
3. C. OTERO AREÁN, A. LÓPEZ BALLÁN, M. PEÑARROYA MENTRUIT, M. RODRÍGUEZ DELGADO and G. TURNES PALOMINO, *Micropor. Mesopor. Mater.* **40** (2000) 35.
4. N. N. GREENWOOD and A. EARNSHAW, "Chemistry of the Elements," 5th edn. (Pergamon Press Ltd. Oxford, 1995) p. 278.
5. S. J. GELLER, *J. Chem. Phys*. **33** (1960) 676.
6. J. FRANK, M. FLEISCHER and H. MEIXNER, *Sensors and Actuators B* **48** (1998) 318.
7. J. FRANK and H. MEIXNER, *ibid.* **78** (2001) 298.
8. M. R. LORENZ, J. F. WOODS and R. J. GAMBINO, *J. Phys. Chem. Solids* **28** (1967) 403.
9. N. UEDA, H. HOSONO, R. WASEDA and H. KAWAZOE, *Appl. Phys. Lett.* **70** (1997) 3561.
10. L. P. SOSMAN, T. ABRITTA, O. NAKAMURA, M. M. F. D'AGUIAR NETO and *J. Mater. Sci. Lett.* **14** (1995) 19.
11. M. HANEDA, Y. KINTAICHI, H. SHIMADA and H. HAMADA, *J. Catal*. **192** (2000) 137.
12. V. KANAZIREV, R. DIMITRIVA, G. L. PRICE, A. YU. KODAKOV, L. M. KUSTOV and V. B. KAZANSKY, *J. Mol. Catal.* **70** (1990) 111.
13. V. KANAZIREV, G. L. PRICE and K. M. DOOLEY, *J. Chem. Soc. Chem Commun.* (1990) 712.
14. P. MERIAUDEAU, G. SAPLAY and NACCACHE, *J. Mol. Catal*. **81** (1993) 712.
15. M. HANEDA, N. BION, M. DATURI, J. SAUSSEY, J. C. LAVALLEY, D. DUPREZ and H. HAMADA, *J. Catal*. **206** (2002) 114.
16. M. MIZUNO, T. YAMADA and T. NOGUCHI, *Yogyo Kyokaishi* **83** (1975) 175.
17. J. M. GALLARDO AMORES, V. SÁNCHEZ ESCRIBANO, G. BUSCA, E. FERNÁNDEZ LÓPEZ and M. SAIDI, *J. Mat. Chem.* **11** (2001) 3234.
18. V. SÁNCHEZ ESCRIBANO, E. FERNÁNDEZ LÓPEZ, SANCHEZ HUIDOBRO, M. PANIZZA, C. RESINI, J. M. GALLARDO AMORES and G. BUSCA, *Solid State Sci.* in press.
19. A. R. WEST, "Solid State Chemistry and Its Applications," (Chichester, Wiley, 1997).
20. J. A. NOH and J. A. SCHWARTZ, *J. Coll. Interf. Sci.* **27** (1986) 531.
21. A. V. NOVOSSELOV, G. V. ZIMINA, A. A. FILARETOV, O. A. SHLYAKHTIN, L. N. KOMISSAROVA and A. PAJACZKOVA, *Mater. Res. Bull*. **36** (2001) 1789.
22. J. M. GALLARDO AMORES, M. C. PRIETO, V. SÁNCHEZ ESCRIBANO, C. CRISTIANI, M. TROMBETTA and G. BUSCA, *J. Mater. Chem.* **7** (1997) 1887.
23. A. CORNELIS-BENOIT, *Spectrochim. Acta.* **21** (1965) 623.
24. E. SCHWARZMANN and H. SPARR, *Z. Naturforsch. Teil B* **24** (1969) 8.
25. J. M. GALLARDO AMORES, V. SÁNCHEZ ESCRIBANO and G. BUSCA, *J. Mater. Chem.* **9** (1999) 1161.
26. M. C. STEGMANN, D. VIVIEN and C. MAZIERES, *Spectrochim. Acta Part A* **29** (1972) 1653.
27. P. G. HALL, H. S. CLARKE and S. C. P. MAYNARD, *J. Phys. Chem*. **99** (1955) 5666.
28. F. A. COTTON and G. WILKINSON, "Advanced Inorganic Chemistry," 4th ed. (J. Willey and Sons, Inc. New York, 1980) p. 444.
29. S. J. WILSON and J. D. C. MCDONNELL, *J. Solid State Chem*. **34** (1980) 315.
30. R. S. ZHOU and R. L. SNYDER, *Acta Cryst. Sect. B* **47** (1991) 617.
31. G. BUSCA, V. LORENZELLI, G. RAMIS and R. J. WILLEY, *Langmuir* **9** (1993) 1492.
32. O. MULLER, W. B. WHITE and R. ROY, *Spectrochim. Acta, Part A* **25** (1969) 1491.
33. G. A. DORSEY, *Anal. Chem*. **40** (1968) 971.

34. P. TARTE, *Spectrochim. Acta, Part A* **23** (1967) 2127.
35. V. SÁNCHEZ ESCRIBANO, J. M. GALLARDO AMORES, E. FINOCCHIO, M. DATURI and G. BUSCA, *J. Mater. Chem.* **5** (1995) 1943.
36. W. G. FATELEY, F. R. DOLLISH, N. T. MCDEVITT and F. F. BENTLEY, "Infrared and Raman Selection Rules for the Molecular and Lattice Vibrations" (Wiley, New York, 1972).
37. A. S. BARKER, *Phys. Rev.* **132** (1973) 1474.
38. S. ONARI, T. ARAI and K. KUDO, *ibid.* **16** (1977) 1717.
39. B. SULIKOWSKI, Z. OLEJNICZAK and V. CORTÉS CORBERÁN, *J. Phys. Chem.* **100** (1996) 10323.
40. D. DOHY, G. LUCAZEAU and A. REVCOLEVSCHI, *J. Solid State Chem.* **45** (1982) 180.
41. R. H. FRENCH, *J. Am. Ceram. Soc.* **73** (1990) 477.
42. E. FERNÁNDEZ LÓPEZ, V. SÁNCHEZ ESCRIBANO, M. PANIZZA, M. M. CARNASCIALI and G. BUSCA, *J. Mater. Chem.* **11** (2001) 1891.
43. S. J. GREGG and K. S. W. SING, Academic Press, London (1991).

Received 17 September 2003
and accepted 19 October 2004